Applied Catalysis B: Environmental 123–124 (2012) 324–332

Contents lists available at SciVerse ScienceDirect

Applied Catalysis B: Environmental

journal homepage: www.elsevier.com/locate/apcatb

$LaNiO_3$ as a precursor of Ni/La_2O_3 for CO_2 reforming of CH_4: Effect of the presence of an amorphous NiO phase

Rosa Pereñiguez*, Victor M. Gonzalez-delaCruz, Alfonso Caballero, Juan P. Holgado*

Instituto de Ciencia de Materiales de Sevilla and Departamento de Q. Inorgánica (CSIC-US), Av. Américo Vespucio, 49 41092 Sevilla, Spain

ARTICLE INFO

Article history:
Received 25 January 2012
Received in revised form 19 April 2012
Accepted 27 April 2012
Available online 5 May 2012

Keywords:
Hydrogen
Perovskite
Dry reforming of methane
XAS
Synthesis methods

ABSTRACT

The objective of the present work has been the study of the physico-chemical and catalytic properties of Ni/La_2O_3 catalysts obtained by reduction of four $LaNiO_3$ samples prepared by different methods. The $LaNiO_3$ precursors as well as the resulting Ni/La_2O_3 catalysts, were characterized by scanning electron microscopy (SEM), X-ray diffraction (XRD), X-ray absorption spectroscopy (XAS), temperature programmed reduction and oxidation (TPR, TPO). The catalytic performances of these systems for dry reforming of methane (DRM) were also tested. These samples show different physico-chemical properties resulting from the synthesis method used. The XAS and TPR measurements show that in all four $LaNiO_3$ samples there is, in addition of the crystalline $LaNiO_3$ rhombohedrical phase, a significant amount of an amorphous NiO phase, not detectable by XRD but evidenced by XAS. The amount of this NiO amorphous phase seems to play, together with some other microstructural parameters, an important role in the performance of the Ni/La_2O_3 samples for the DRM reaction.

1. Introduction

In recent years, reaction of the dry reforming of methane (DRM, $CH_4 + CO_2 \rightarrow 2CO + 2H_2$) has stimulated a big scientific interest as a possible way to obtain the so called "synthesis gas" (syngas) with a low H_2/CO ratio. This technological and scientific interest is due, among some other factors, to the possible use of some natural gas reserves where CH_4 is found with big amounts of CO_2. Although some other formulations based on noble metals are very stable and active, catalysts based on nickel as active phase present the best balance between economical cost and catalytic performance. These kinds of catalytic systems are, however, very sensible to deactivation due to the carbon deposition and the improvement of its stability remains an important challenge [1–5]. This kind of carbon deposition can be formed from the catalytic decomposition of CO ($2CO \rightarrow CO_2 + C$) or CH_4 ($CH_4 \rightarrow C + 2H_2$). The first process is favoured at low temperatures, but taking into account that the concentration of CO at low temperatures is expected to be low, the contribution of this reaction to the carbon deposition should be small. On the other hand, at higher temperatures, the decomposition of methane is favoured, where the reforming reaction takes place.

One of the factors that seem to control the stability of these systems is the size of Ni particles. In fact, catalysts where Ni is present as small particles (< 20 nm) show the lower carbon deposition and, hence, better stability. In this context, the preparation method of small Ni particles is a key to obtain better catalysts. In the later years, the so called "solid phase crystallization"(spc), has attracted special attention [6] as a simple and effective method to prepare good catalysts based on small particles of the active metal dispersed on the support. In the case of nickel catalysts, the method starts from an oxide $NiMO_y$ where Ni is homogenously distributed in the structure, from where is "extracted" by reduction of the oxide structure, leading to a Ni/MO_x system. In this context, much attention has been devoted to the possible use of lanthanum-transition metal perovskites ($LaMO_3$) [7–9] for reforming reactions – mainly dry reforming of methane – being especially important the effort dedicated to $LaNiO_3$. In this context, although most of the works indicate, in general, a good catalytic behaviour of the compound $LaNiO_3$, there is still a lot of controversy on aspects such as the reducibility (a key point as reducing step is crucial for obtaining the final catalyst) or the presence of different phases and the size of Ni particles in the active Ni/La_2O_3 phase (formed after reduction). We consider that most of these controversies (found across the literature works [6,10–14]) can be explained in terms of the physicochemical differences resulting from the different preparation methods used for obtaining the $LaNiO_3$ compound. In a previous paper [15] we have studied that the reduction of $LaNiO_3$ "perovskite" prepared by spray pyrolysis, results in a metallic Ni phase supported over La_2O_3, either using a previous reduction step

* Corresponding authors.
E-mail addresses: rosa@icmse.csic.es (R. Pereñiguez), holgado@icmse.csic.es (J.P. Holgado).

0926-3373/$ – see front matter © 2012 Elsevier B.V. All rights reserved.
http://dx.doi.org/10.1016/j.apcatb.2012.04.044

or even during exposure to reactants atmosphere ($CH_4 + CO_2$). It is important to mention that although reduction (decomposition) of $LaNiO_3$ phase for production of the Ni/La_2O_3 catalyst is generally accomplished in a previous stage, there are several works [12–16] that refer that heating the $LaNiO_3$ phase in the reactive gases ($CO_2 + CH_4$) causes also the decomposition towards Ni/La_2O_3, leading to systems with better performance if compared with those obtained by pre-reduction in hydrogen atmosphere. Using Ni/La_2O_3 for DRM, Zhang and Verykios [17] detected the presence of the $La_2O_2CO_3$ phase after reforming reaction decorating the Ni particles, playing a precise role for avoiding the deactivation of this kind of catalyst.

In a previous work [15], we have found that the "original" system ($LaNiO_3$ calcined) is not a single phase, but a mixture of a $LaNiO_3$-crystalline phase (well detected by X-ray diffraction – XRD) together with a NiO-amorphous phase, which was only detected by X-ray absorption spectroscopy (XAS). The existence of this type of phase was suggested by Ruckenstein and Hu [10] more than a decade ago, and has been detected as a trace in the XRD diffractograms, as reported in few papers [11,13]. Nevertheless, the presence of this NiO phase as a significant contribution under calcination conditions not far from those found in many papers has only been confirmed by us using XAS [15].

Based on those previous results for the sample prepared by the method of spray pyrolysis, we decided to explore if the NiO phase was also present in other $LaNiO_3$ samples prepared by different methods. We have chosen four methods to prepare the $LaNiO_3$ precursor, characterizing them by several complementary techniques, studying the presence of the NiO amorphous phase and comparing the reactivity for dry reforming of the Ni/La_2O_3 formed after reduction. Our goal is to determine the effect of the synthesis in the physico-chemical properties of the $LaNiO_3$ as a precursor of the Ni/La_2O_3 catalysts and their activity for carbon dioxide reforming of methane.

2. Experimental

2.1. Catalyst preparation

The lanthanum nickel perovskite $LaNiO_3$ was prepared by the following methods: hydrothermal synthesis (HT), combustion (CM), spray pyrolysis (SP) and spray pyrolysis-combustion (SPCM), a combined method proposed by us, and schematized in Fig. 1.

In the hydrothermal synthesis ($LaNiO_3$-HT), the precursors $La(NO_3)_3$ (3 mmol), $Ni(NO_3)_2$ (3 mmol) and citric acid (3 mmol) were dissolved in the minimum amount of water and this solution was added to another one prepared with CTAB (2.33 g of cetyltrimethylammonium bromide, CTAB, used as surfactant) dissolved in 60 ml of distilled water and 10 ml of HCl 10%. This solution was mixing all together with a magnetic stirrer at R.T. during at least 2 h. After that, 40 ml of a solution of NaOH 1.5 M is added, with further stirring for 6 h. This step increases the pH of the solution and induces the precipitation of an intermediate product. The suspension formed is placed in a stainless-steel autoclave reactor, with a Teflon vessel in the inner part, which is heated in an oven (503 K) during 24 h. The solid obtained was centrifuged and washed (until neutral pH is detected in the rinsing water), dried in air and finally calcined in flowing synthetic air, at 873 K for 4 h [18].

In the combustion ($LaNiO_3$-CM) method we start from an aqueous solution of an equimolar mixture of La and Ni nitrates (7 mmol) that are mixed with a convenient amount of citric acid (8 mmol), according with parameters described previously for this type of synthesis and compounds [19–21]. Initially the dissolution is gently heated in a plate to evaporate most of the water, forming a gel that is further heated to obtain an almost dried powder. Then the temperature of the plate is quickly increased, what results in an auto-combustion reaction. The powder obtained after this combustion is also calcined at 873 K to eliminate possible carbonaceous impurities.

$LaNiO_3$ was prepared by spray pyrolysis using the experimental setup described elsewhere [22]. Briefly a solution containing nitrates of all the elements is introduced in the reactor as a "mist" or a spray, by means of an ultrasonic transductor. Once the aerosol is obtained, it is transported through the reactor (in an air atmosphere), forced by a suction pump located at the end of the system. In our case, the reactor consists of a quartz tube divided into two independent temperature zones that were controlled at 523 K (drying) and 873 K (decomposition) respectively. $LaNiO_3$ perovskite was prepared from a solution containing $La(NO_3)_3$ and $Ni(NO_3)_2$ with a concentration of 0.05 M each. Particles of synthesized material are collected in a funnel with a porous frit, heated at ca. 373 K to avoid its physical blocking. Finally, the solid is dried in an oven at ca. 423 K and calcined in air at a temperature equal to that of decomposition furnace (873 K).

Finally, spray pyrolysis-combustion ($LaNiO_3$-SPCM) method uses the same setup as $LaNiO_3$-SP, but citric acid is added to the precursor solution, in a similar ratio metal nitrates:citric acid, than in the combustion method ($LaNiO_3$-CM). The powder obtained was calcined in air at 873 K for 4 h.

An additional sample of Ni supported over La_2O_3 with a comparable metallic load (26 wt%Ni/La_2O_3) was prepared by impregnation of a La_2O_3 (prepared by combustion as $LaNiO_3$-CM) with a nickel nitrate solution. The system obtained was also calcined in air at 873 K for 4 h. This last sample was prepared as a reference for some characterization techniques.

In all the cases the reactants were purchased from Sigma–Aldrich, Merck or Fluka, with a purity of at least 99% and used as received.

2.2. X-ray diffraction (XRD)

X-ray diffractograms, were recorded in a Siemens D-500 equipment, with a Bragg–Brentano configuration, using Cu Kα ($\lambda = 1.5418$ Å). Spectra were collected in the range $2\theta = 20–80^\circ$, with a step of 0.05° and an acquisition time of 1 s for each point. Particle size values were calculated by means of the Scherrer equation applied for $LaNiO_3$ to the (2 0 2) plane at $2\theta = 33^\circ$ (the main peak of the $LaNiO_3$ at $2\theta = 47.3^\circ$ corresponds to a doublet, being not well resolved), and for Ni^0 to the (1 1 1) plane at 44.5°.

2.3. Scanning electron microscopy (SEM) and BET specific surface area measurements

Scanning electron microscopy (SEM) images were obtained in a Hitachi S-5200 microscopy, with a field emission filament, using an accelerating voltage of 4–5 kV, and an extraction current of 10 μA.

Specific surface areas were determined by BET isotherms carried out with N_2 adsorption–desorption curves at 77 K in a Micromeritics model ASAP 2010. The samples were previously degassed at 473 K for 2 h.

2.4. X-ray absorption spectroscopy (XAS)

X-ray absorption spectra were recorded at the SuperXAS beamline of the SLS synchrotron (Villigen, Switzerland) and BM-25 beamline of the ESRF synchrotron (Grenoble, France). The spectra corresponding to "ex situ" prepared samples were all acquired in transmission mode, being the pellets prepared using the optimum weight to maximise the signal-to-noise ratio in the ionisation chambers ($\log I_0/I_1 \approx 1$) and mixed with BN. For energy calibration, a standard Ni foil was introduced after the ionisation chamber

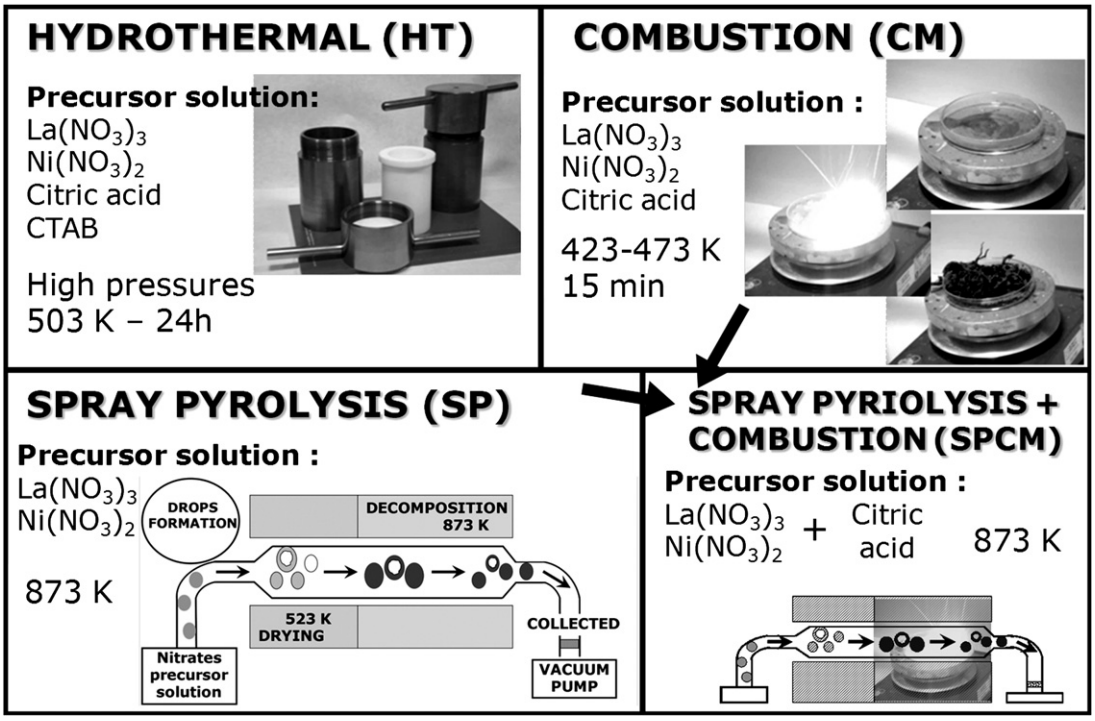

Fig. 1. Schematic summary of the four methods used for $LaNiO_3$ preparation.

(I_1) and measured simultaneously. Typical XAS spectra of Ni K edge were recorded from 8230 eV to 9190 eV, with a variable step energy value, with a minimum 0.5 eV step across the XANES region (8315–8375 eV). EXAFS spectra were analysed using the analysis package ATHENA [23], with the theoretical amplitude and phase shift functions proposed by Ankudinov and Rehr (version 7.02 [24]) (being only corrected the phase shift of the absorbing atom). Reference spectra for Ni and NiO were recorded using standard reference samples. For the $LaNiO_3$, a reference spectrum was taken from the literature [25]. The data presented later correspond just to the EXAFS spectra (whose oscillations were Fourier transformed), so we are going to refer to these results as EXAFS from here after.

2.5. Temperature programmed reduction (TPR)

Temperature programmed reduction (TPR) experiments were done according to the experimental conditions described elsewhere [26] to avoid coalescence of the peaks and optimization of the signal, using 12 mg of $LaNiO_3$. A H_2/Ar mixture (5% H_2, 50 ml/min flow) was used as the reducing atmosphere from room temperature up to 1073 K, with a heating rate of 10 K/min. A thermal conductivity detector (TCD), previously calibrated using CuO, and a mass spectrometer in line with the TCD, calibrated with reference mixtures, were used to detect variations of H_2 concentration, and, in the case of mass spectrometer, to record possible sub-products formation.

2.6. Catalytic activity tests: dry reforming of methane (DRM)

Reaction was carried out in a tubular reactor ("U" shaped), using 20 mg of catalysts between two pompons of quartz wool. The samples were pre-treated in a flow of 50 ml/min H_2 (5%)/Ar mixture at 1073 K for 1 h, to reduce the $LaNiO_3$ to a system based in Ni/La_2O_3. The CH_4 and CO_2 reactants (with the ratio 1:1) were diluted in He (9:9:82 in volume). Samples of $LaNiO_3$ pre-reduced in contact with the reaction mixture were heated from room temperature up to 1073 K at 1 K/min rate, holding the samples at 1073 K during 12 h, and cooled down to room temperature in the same reaction mixture.

Reactants and products were analysed using a gas chromatograph (Varian, GC-3800) equipped with a thermal conductivity detector (TCD), and two columns with an "in line" configuration (Molecular Sieve 5 Å, Porapak®-N).

The $T^{50}_{CH_4}$ values, shown in Figs. 6 and 9, are defined as the temperature at which 50% conversion of CH_4 is achieved.

3. Results and discussion

3.1. Catalysts characterization

3.1.1. X-ray diffraction

Fig. 2 presents the XRD diffractograms of the $LaNiO_3$ calcined at 873 K, prepared by the four methods (left), together with those of the samples after the treatments of reduction at 1073 K (right) for studying the state of the metallic active phase (Ni^0). Comparison of the diffractograms of the original calcined samples with $LaNiO_3$ phases in ICDD 2000 database [27], allows us to assign the peaks at 23.2°, 47.3° and 33° to a rhombohedral (R-3m) structure as the main phase in the four systems. Although the peak at 33° is not completely resolved, assignment to rhombohedral phase is reinforced by the ratio of intensities of peaks at 41° and 47.3°. Besides the perovskite phase, it has been found a minor contribution of tetragonal La_2NiO_4 and cubic NiO phases in the sample prepared by combustion but not detected in any other sample. By applying the Scherrer equation to the calcined systems at peak 47.3° (2 0 2), we obtained the values of the $LaNiO_3$ primary crystallite size shown in Table 1, that are in the order of 12–19 nm, except for the one prepared by SP, relatively bigger (32 nm).

The reduction of these "niquelites" ($LaNiO_3$) resulted in Ni^0/La_2O_3 samples in all the cases, where the metallic phase of Ni showed a cubic structure and La_2O_3 an hexagonal phase. In this case, the results of Scherrer equation (Table 1) reveal different sizes for the Ni crystallite (1 1 1), following the trend: HT < SPCM < CM < SP. It is important to mention, that the Ni

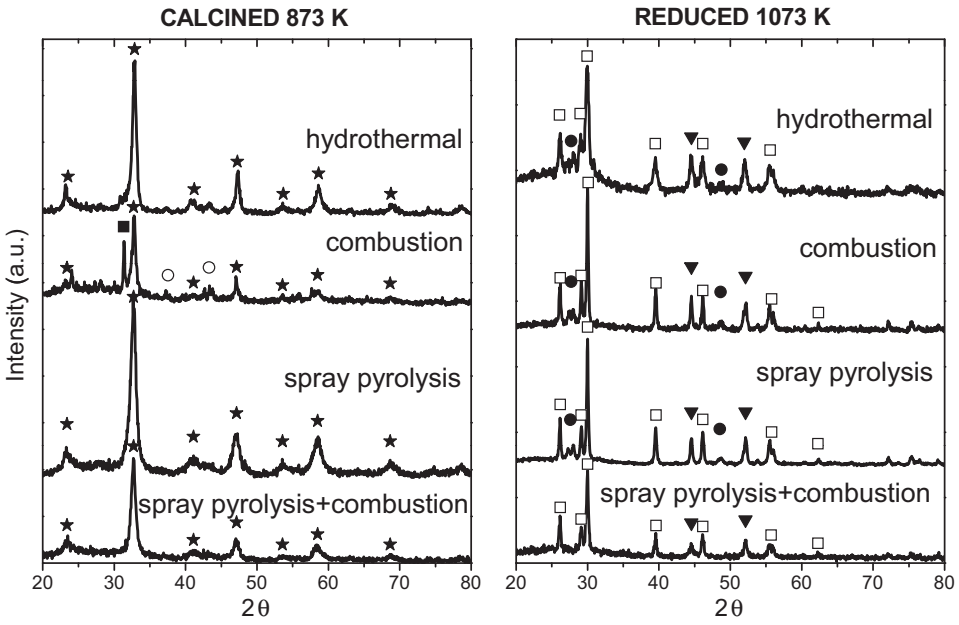

Fig. 2. XRD diagrams of the $LaNiO_3$ samples (HT, CM, SP and SPCM) after calcination (left) and reduction (right). Diffraction patterns: left—(⋆) $LaNiO_3$-rhombohedral; (■) La_2NiO_4-tetragonal; (○) NiO-cubic. Right—(▼) Ni-cubic; (□) La_2O_3-hexagonal; (●) $La(OH)_3$-hexagonal.

crystallite size has been reported [28,29] as one determinant factor for the reforming activity and the degree of coke deposition together with faces exposed preferentially on those Ni^0 particles. One of the routes to form the carbon deposition is due to the disproportionation of CO (a product of the reforming of methane) through the Boudouard reaction ($2CO \rightarrow C + CO_2$). In this context, it has been reported [30–33] that some steps of this reaction, (dissociation of CO) involve Ni—Ni ensembles [34], formed by 4–6 atoms of Ni as active sites. In the reaction of dry reforming, the main step is the activation of methane that occurs through the CH activation over a single metal atom [35,36]. Depending on how the reaction rate varies as a function of the particle size, methane activation is the prototype reaction of class II type behaviour [34,37], which shows a uniform increase in reaction rate with decreasing particle size. This tendency to a bigger reactivity in smaller particles must be balanced with the higher deposition of carbon in small particles [38,39] giving as a result the objective of obtain a compromise situation for the optimum size for Ni particles, that seems to be ca. 10–20 nm [40].

3.1.2. Scanning electron microscopy and BET specific surface area measurements

The SEM images of $LaNiO_3$ prepared by each method after calcination at 873 K are presented in Fig. 3. It can be seen that the samples prepared by hydrothermal and combustion methods are morphologically very similar, formed by agglomerates of particles with a size of 40–80 nm. In contrast, the sample synthesized by spray pyrolysis ($LaNiO_3$-SP) shows pseudo-spherical particles, with a variable size of 150–500 nm, constituted by aggregates of smaller nanoparticles (20–40 nm). This is in concordance with the bigger size calculated by Scherrer equation for $LaNiO_3$-SP XRD (see Table 1). Finally, the $LaNiO_3$-SPCM has a similar morphology to the $LaNiO_3$-SP, consisting in pseudo-spherical particles of ca. 300 nm to 1 μm. It is here important to incise that the size of the particles (for the samples SP and SPCM) is related with the initial step of the preparation method, where solution drops are formed by nebulizer at the entrance of the reactor, where they are decomposed to form the perovskite. Nevertheless, the difference between $LaNiO_3$-SP and $LaNiO_3$-SPCM is the acid citric added to the precursor solution that causes a microscopic "combustion" process on each particle. This combustion process includes the formation of considerable amounts of gaseous products inside the solid particles, giving a more porous character to the sample, but also in an extra heat transfer due to the exothermic character of the combustion process, resulting also in the formation of smaller well defined nanoparticles that can be clearly observed in the surface of the agglomerates for the $LaNiO_3$-SPCM sample. This higher porosity is reflected in the high value of specific surface obtained for this sample, as we can see in Table 1. In this table is presented the results of specific surface obtained by BET, which varies from 4.2 m^2/g for the $LaNiO_3$-SP to 16.6 m^2/g obtained for the $LaNiO_3$-SPCM. Although these values are comparable with the ones found

Table 1
Crystallite size (calculated by XRD-Scherrer), BET surface area of $LaNiO_3$ and H_2 consumptions calculated from TPR experiments.

Synthesis methods: $LaNiO_3$	Crystallite size^{XRD} (nm)		Surface	Consumption of H_2 (TPR)	
	$LaNiO_3$ (2 0 2) $\theta = 47^\circ$	Ni^0 (1 1 1) $\theta = 44.5^\circ$	BET (m^2/g)	H_2 uptake ($mmol^{H_2}/g^{catalyst}$)	Δn^+
	Air – 873 K	H_2 – 1073 K	Air – 873 K	Air – 873 K	
HT	19	19	9.9	5.3	2.6
CM	19	42	4.7	4.4	2.2
SP	32	69	4.2	5.9	2.9
SPCM	12	30	16.6	5.6	2.7

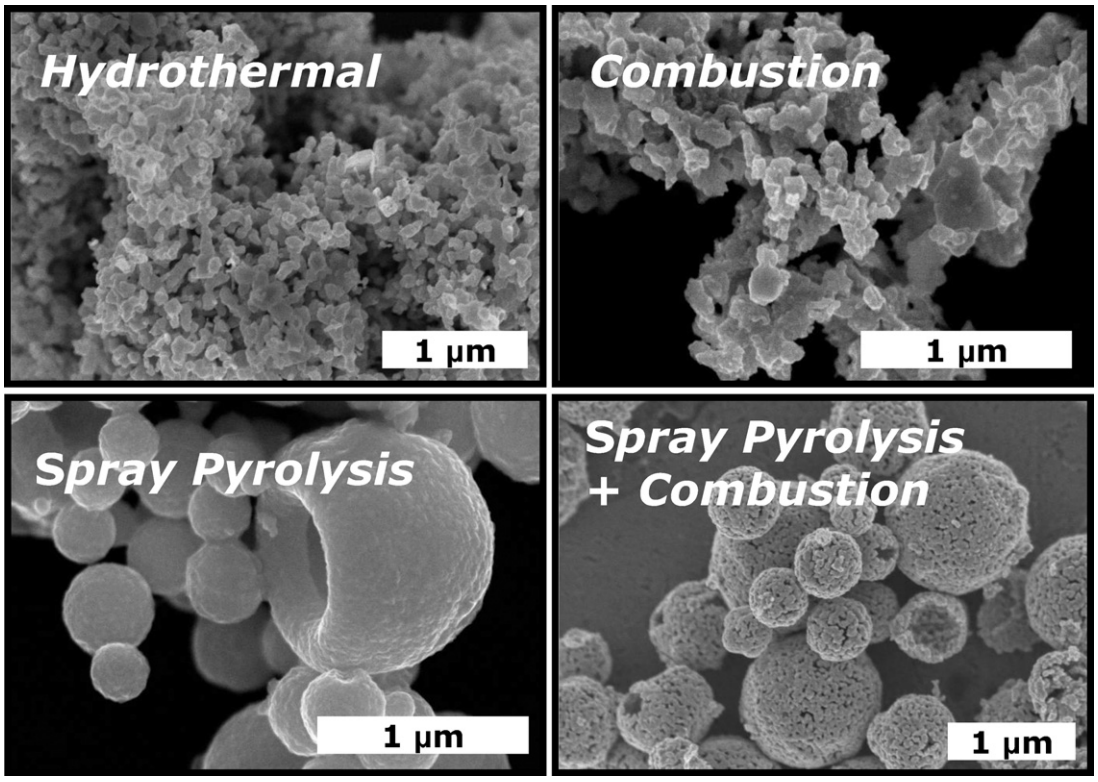

Fig. 3. SEM images of the $LaNiO_3$ samples (HT, CM, SP and SPCM) after calcination in air at 873 K.

in the literature for this kind of materials [7,13,16,41,42] calcined in the same range of temperatures, the result obtained for the $LaNiO_3$-SPCM is significantly higher, probably due to the existence of well crystallized nanocrystals previous to the calcinations process, which may inhibit the sintering process.

3.1.3. *EXAFS characterization of samples $LaNiO_3$*

Fig. 4 shows the Fourier transforms (FTs) of the EXAFS oscillations of the Ni K edge of $LaNiO_3$ samples prepared by SP, SPCM, HT and CM after calcination in air at 873 K for 4 h. The most significant data of the FT of Ni, NiO references and a well characterized $LaNiO_3$ sample [25] have been incorporated in a table on the top of Fig. 4. FTs of the four prepared $LaNiO_3$ samples present three main peaks, centred at ca. 1.8 Å, 2.8 Å and 3.3 Å (with a shoulder at 3.8 Å). Taking into account that these values correspond to an analysis without a complete phase shift correction, a simple comparison with the references clearly reveals that the peaks at 1.8 Å and 3.3 Å, could be assigned to a perovskite phase, corresponding to the distances Ni—O (1.9 Å) and Ni—La (3.4 Å) respectively in the perovskite structure, with a shoulder at 3.8 Å ascribed to the distance Ni—O—Ni in the perovskite.

However the peak at 2.8 Å, does not correspond to any $LaNiO_3$ distance, but clearly appears in the same position as the Ni—Ni coordination shell in the NiO-reference (2.9 Å). As previously reported by us [15], this peak corresponds to a second phase, consisted of NiO. Moreover, because this phase is not observed by XRD (Fig. 2) it should be mostly formed by amorphous and disordered particles. This NiO phase would also contribute to the peak observed at 1.8 Å, ascribed to the distance Ni—O at 1.9 Å (see Table of references in Fig. 4). A more detailed discussion of this assignment of the amorphous phase can be found in a previous work of us [15]. From here after, we are going to mention the peaks referred to the values with complete phase shift correction (Table in Fig. 4).

Although a detailed fitting process has not been performed, due among other factors to the elevated error associated with so many coordination spheres, is possible to make an approximation of the proportion of the $LaNiO_3$ and NiO phases present in the four samples, from the relation between the intensities of the peaks at 2.9 Å (NiO) and 1.9 Å ($LaNiO_3$ + NiO) (I^{peak2}/I^{peak1}), although this proportion should be taken not as an absolute value but for comparative purposes only. These ratios (I^{peak2}/I^{peak1} or NiO/$LaNiO_3$

REFERENCES	$LaNiO_3$			NiO		Ni
Coordination shell	Ni-O	Ni-La	Ni-O-Ni	Ni-O	Ni-Ni	Ni-Ni
C.N.	6	8	6	6	12	12
D (Å)	1.9	3.4	3.8	1.9	2.9	2.5

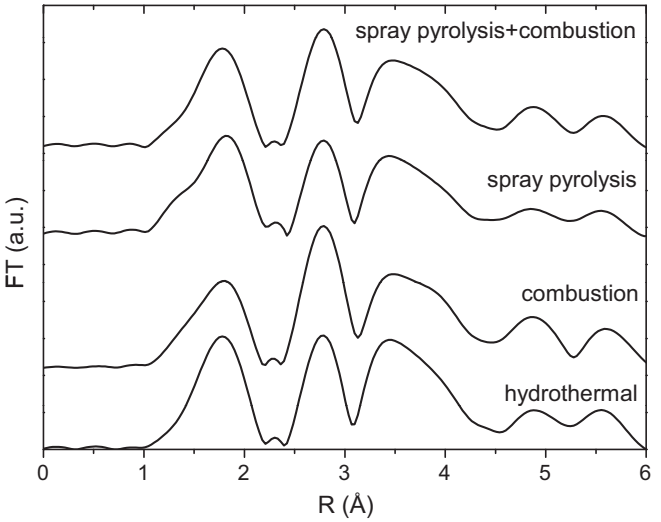

Fig. 4. FTs. of the Ni K-edge EXAFS spectra obtained for the $LaNiO_3$ samples (HT, CM, SP and SPCM) after calcination at 873 K. $LaNiO_3$ [25], NiO and Ni references are also included as a table.

Table 2
Relations between the intensity of the FTs obtained for the samples $LaNiO_3$ prepared by HT, CM, SP and SPCM after the treatments indicated (I^{peak2}/I^{peak1} and I^{peak3}/I^{peak1}).

Synthesis methods and treatments	$I^{peak2}/I^{peak1} \sim$ NiO/$LaNiO_3$			$I^{peak3}/I^{peak1} \sim$ structural order		
Gas mixture	Air	O_2 (3%)	O_2 (100%)	Air	O_2 (3%)	O_2 (100%)
Temperature (K)	873	1073	1073	873	1073	1073
Hours	4	3	24	4	3	24
HT	1.0	0.9	~0.3	1.0	1.1	1.2
CM	1.6	1.0	~0.2	1.1	1.1	0.9
SP	0.9	0.5	~0.2	0.8	1.0	1.0
SPCM	1.2	1.0	~0.4	0.9	1.1	1.0

phase ratio) are collected in Table 2 which shows that the $LaNiO_3$-CM presents the biggest proportion of NiO, while the other three samples have similar NiO/$LaNiO_3$ ratio with slight differences following the order: SPCM > HT > SP. Using a similar approach, and considering the fact that not well crystallized $LaNiO_3$ would have an intensity of the peak at 3.3 Å smaller than the reference spectrum (well defined $LaNiO_3$ phase, Table in Fig. 4) an estimation of the structural order of the phase $LaNiO_3$ can be also estimated from the intensity of the second sphere of the perovskite at 3.3 Å in relation with the intensity of the first one (I^{peak3}/I^{peak1} also shown in Table 2), although this estimation should be used only for comparative purposes. It is noteworthy that these ratios have comparable values for the four systems which uncover a similar crystallinity for the $LaNiO_3$ phase in the samples tested (at least after their first calcination treatment, see further in the text the effect of the concentration of oxygen and the temperature in others calcinations treatments).

3.1.4. Temperature programmed reduction (TPR)

The reducibility of the calcined NiO + $LaNiO_3$ samples versus temperature (TPR) has been tested, being the results collected in Fig. 5. The profiles for a pure NiO and a NiO/La_2O_3 sample prepared by impregnation have been also included in Fig. 5 for reference purposes.

The four $LaNiO_3$ samples "as-calcined" present two broad processes of reduction. The maximum of the first process varies, depending on the synthesis method, from 623 K to 723 K, a temperature close to the bulk NiO reduction peak (ca. 673 K). Meanwhile, the maximum temperature of the second process of reduction lies within a 25 K range (793–818 K), appearing the maxima in the sequence: SPCM → HT → CM → SP.

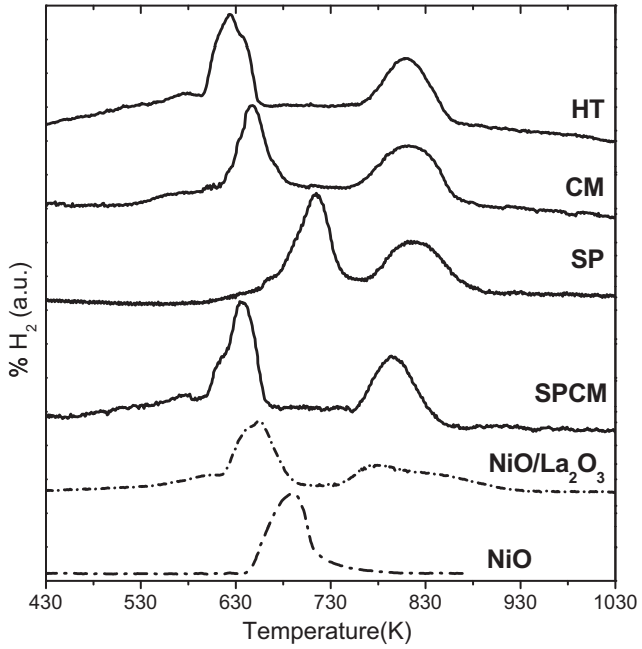

Fig. 5. Temperature-programmed reduction (TPR) profiles of the $LaNiO_3$ samples (HT, CM, SP and SPCM) and NiO/La_2O_3 (impregnation) after calcination in air at 873 K. TPR of bulk NiO is also included as a reference.

It should be noted that as discussed in a previous work [15] and also in Section 3.1.3, the presence of a significant amount of an amorphous NiO phase has been clearly evidenced by us. On that basis, we have assigned the first peak of the reduction profiles, at low temperatures, initially to the reduction of the NiO phase to Ni^0 and the second peak, at higher temperatures, to the reduction of the $LaNiO_3$ phase.

Moreover, a controversy in the assignation of these two peaks exists in the literature, summarized as hypothesis A and B:

	Hypothesis A	Hypothesis B
Process 1 623–723 K	$NiO + H_2 \rightarrow Ni + H_2O$	$LaNiO_3 + H_2 \rightarrow La_2Ni_2O_5$, La_2NiO_4
Process 2 793–818 K	$2LaNiO_3 + 3H_2 \rightarrow 2Ni + La_2O_3 + 3H_2O$	$La_2Ni_2O_5$, $La_2NiO_4 + H_2 \rightarrow Ni + La_2O_3$

Most of the authors [11,12,43] support the assignation B, where the reduction of $LaNiO_3$ is the only process but takes place in two steps. In the first one (low temperature) the Ni^{3+} in the perovskites reduces to a phase based in Ni^{2+} ($La_2Ni_2O_5$, La_2NiO_4). This step would be followed by a second reduction process at higher temperature, where the Ni^{2+} reduces to metallic Ni^0. On the other hand, Ruckenstein and Hu [10] (possibility A), proposed more than a decade ago, two different phases/processes of reduction; in the first one an amorphous phase based on Ni^{2+} (NiO) reduces to Ni^0 and in the high temperature reduction, $LaNiO_3$ reacts with the H_2 to form directly Ni^0 over La_2O_3. This model has been also supported more recently by Guo et al. [14]. Nevertheless, it should be remarked that in both works the authors did not present any evidence of the presence of the NiO phase.

The values of H_2 consumption determined from the TPR profiles and the equivalent change in oxidation state of the reducible phase (Δn^+) are presented on Table 1. Even considering a margin of error of about 10%, these values can be used to study the amount of NiO (2^+) and $LaNiO_3$ (3^+) present in the samples. As can be observed, the H_2 consumption in TPRs for the four samples are lower than the theoretical value (6 $mmol^{H_2}/g^{catalyst}$), which can be related with an incomplete reduction of an Ni^{3+} or with a complete reduction of a mixture of phases Ni^{2+}/Ni^{3+}. Taking into account the presence of NiO phase (detected by EXAFS) and that the characterization of the samples after reduction in the same conditions (by XRD Fig. 2 right and EXAFS not shown) reveal a complete reduction of the Ni^{n+} phase, we can dismiss the first possibility. In a previous paper [15] we have already estimated for the reduction of $LaNiO_3$-SP, that a value of $\Delta n^+ = 2.9$ is compatible with the presence of about 10% of nickel in the form Ni^{2+} (NiO). The Δn^+ must be lower for higher NiO/$LaNiO_3$, being $\Delta n^+ = 3$ when the perovskite is pure. If we compare the values obtained by TPR (Table 1) with the estimated NiO/$LaNiO_3$ ratio using EXAFS data (Table 2), we can observe

$LaNiO_3$ reduced (20mg)	H_2/CO	T_{CH4}^{50} (K)
▲ **Hydrothermal**	1.00	903
■ **Combustion**	0.63	-
▷ **Spray pyrolysis**	0.87	1040
○ **Spray pyrolysis+Combustion**	0.99	885

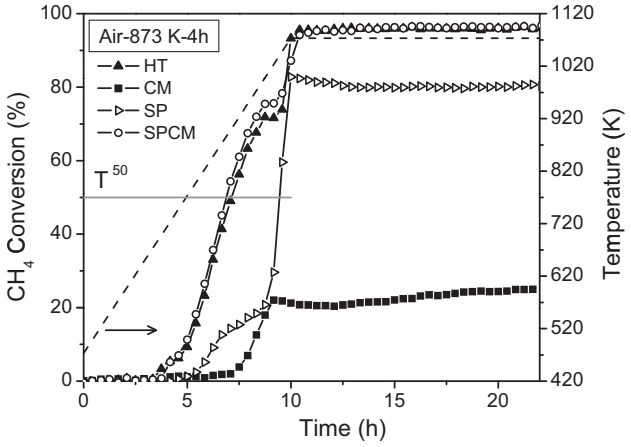

Fig. 6. CH_4 conversion, H_2/CO at 1073 K (t = 12 h) and temperature at 50% of CH_4 conversion ($T_{CH_4}^{50}$) for $LaNiO_3$ catalysts pre-reduced.

that both estimations point out a similar tendency in the amount of NiO amorphous phase (CM ≫ SPCM ∼ HT > SP).

It is important to mention that due to the global stoichiometry of the compounds, together with the NiO phase, there should be also a La_2O_3 amorphous phase not detected by XRD neither affected by reduction processes. In systems $MO/M'O_x$ similar to that here (NiO/La_2O_3), a lower temperature of reduction could be related with a bigger dispersion of the minority phase on the support [44], also sustained with the higher temperature of reduction obtained for the bulk NiO. Fig. 5 shows that the maximum of the first reduction peak (NiO → Ni) presents an increase of the temperatures following the order: *HT* < SPCM < CM < SP. Following our assumption, the samples would present different dispersion of the particles NiO onto the La_2O_3 support, being higher in the HT and SPCM samples, followed by CM and SP samples.

3.1.5. Catalytic activity in DRM

As we detailed in the experimental section, the four $LaNiO_3$ samples were tested, under diluted conditions, for DRM reaction. The results of conversion and products formation are collected in the Fig. 6. As the conversion of methane plots reveal, the systems synthesized by HT and SPCM present the best catalytic performances, followed by the system SP, with 80% of methane conversion. These three catalysts have also a good stability during 12 h of reforming, with some differences between them in conversion and selectivity that we will discuss later. The $LaNiO_3$ prepared by combustion presents the more distinct behaviour of all, having much lower conversion and a lower H_2/CO ratio nearby 0.6, significantly smaller than other samples where this ratio is ca. 1.0. Taking this data in consideration, the general trend in the catalytic activity increases in the following order: HT ≈ SPCM > SP ≫ CM. This tendency is also the same for H_2/CO ratio values. It is important to remember that a H_2/CO ratio lower than 1 represents a higher conversion of CO_2 compared with CH_4, indicating that the reverse water gas shift reaction ($CO_2 + H_2 \rightarrow CO + H_2O$) takes place at the same time than the reforming of CH_4. This undesired reaction would take place for the $LaNiO_3$-SP and especially in the $LaNiO_3$-CM samples. It is also interesting to note that a similar tendency to that observed for the conversion and the H_2/CO ratio has been detected between the

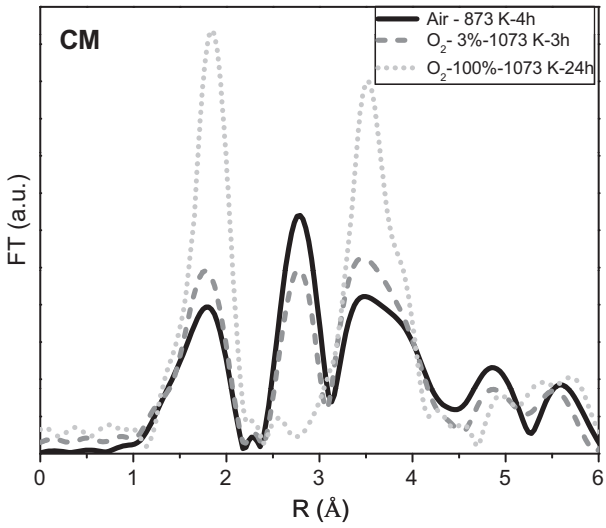

Fig. 7. FTs. of the Ni K-edge EXAFS spectra obtained for the $LaNiO_3$-CM after treatments: (a) air 873 K, 4 h; (b) O_2 (3%)–He 1073 K, 3 h and (c) O_2 (100%) 1073 K, 24 h.

samples SP, HT and SPCM, with respect to the temperature where 50% conversion is obtained (T^{50}). This T^{50} corresponds to ca. 890 K for $LaNiO_3$-SPCM and $LaNiO_3$-HT, and 1040 K for the $LaNiO_3$-SP (see Fig. 6), following a tendency SPCM ≈ HT < SP < CM (not reached).

Although the reactivity and performance of a catalyst is governed by a complex set of factors, and we have not found an unique parameter that seems to control uniquely the catalytic performance and stability, from these experimental results it can figure out some of the factors controlling the catalytic performance. So, according to the previous results, it seems that samples with higher surface area (SPCM and HT), smaller size of the $Ni^0_{Scherrer}$ (HT and SPCM) and higher dispersion of the NiO over the support (HT and SPCM) present better catalytic performances.

Nevertheless, the amount of NiO amorphous phase (lower in the samples SP, HT and SPCM) seems to play an important role; permitting to explain the intermediate performance of the $LaNiO_3$-SP sample (with low NiO content but big Ni particles and bad dispersion) and the poor performance of the $LaNiO_3$-CM one (with the bigger NiO content and intermediate values in the Ni size, dispersion, and surface area).

3.2. Effect of calcination treatments

In view of the fact that the amount of NiO phase seems to be an important factor, we decided to study the effect of further calcinations in this amount of NiO on the different samples and its influence on the catalytic performance. In this part of the study and due to the amorphous character of the NiO phase we have followed its evolution by EXAFS, paying also attention to the TPR profiles, to find its correlation with the EXAFS data.

3.2.1. EXAFS characterization

Samples were submitted to two further calcination treatments under oxidative atmosphere: O_2 diluted (3% – He) at 1073 K during 3 h (higher temperature than previous one) and pure O_2 (100%) at 1073 K during 24 h (longer time, higher concentration of O_2). Fig. 7 shows the FTs after the different oxidation treatments of the $LaNiO_3$-CM sample as an example where some changes are reflected. Firstly, the most remarkable fact is how the peak centred at 2.9 Å (ascribed to NiO) is getting lower with the further oxidation treatment, indicating that this amorphous phase of NiO is disappearing under these conditions. Moreover, the third peak centred at ca. 3.3 Å, for the samples calcined in air at 873 K, presents a

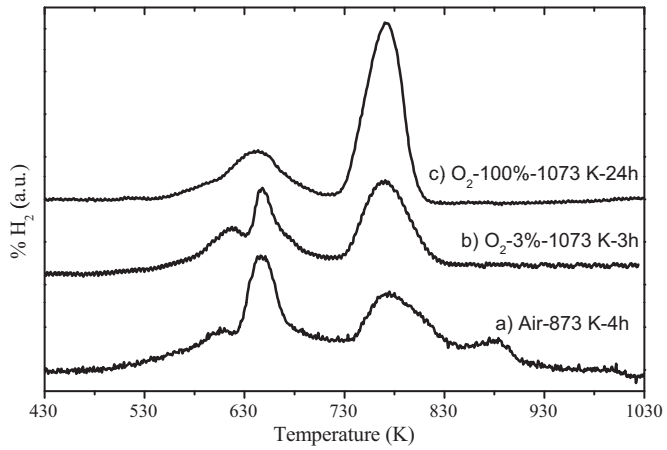

Fig. 8. Temperature-programmed reduction (TPR) profiles of the $LaNiO_3$-CM after treatments: (a) air 873 K, 4 h; (b) O_2 (3%)–He 1073 K, 3 h and (c) O_2 (100%) 1073 K, 24 h.

considerably width and an asymmetrical shape, with a clear shoulder appearing at bigger distances. These features are probably related to two coordination shells being ascribed to the distances Ni—La (3.4 Å) and the shoulder Ni—O—Ni (3.8 Å) in the perovskite structure. After the oxidizing treatment (O_2 – 100%) the shape of this peak gets more resolved in the four samples (see Fig. 7 of $LaNiO_3$-CM sample as an example), which could be also related with an enhancement in the niquelite phase versus NiO, that involve a smaller overlapping of the disappeared peak ascribed to NiO phase.

The Table 2 shows the ratios of the intensities for peaks: I^{peak2}/I^{peak1} and I^{peak3}/I^{peak1}, of the FTs for the niquelites prepared by the four methods previously calcined in air at 873 K and after the cited treatments. The results show how the proportion of the amorphous NiO phase decreases gradually (air–873 K → O_2–3%–1073 K → O_2–100%–1073 K) after the oxidation treatments in the four samples. Taking into account the values of these two ratios (lower I^{peak2}/I^{peak1} and slightly higher I^{peak3}/I^{peak1}) we can follow how the formation of the pure perovskite is completed by increasing the temperature of calcinations and using a more oxidative atmosphere.

3.2.2. TPR and DRM: studies of the $LaNiO_3$-combustion sample

The $LaNiO_3$ prepared by combustion (calcined at 873 K) was the sample that presents a bigger contribution of the NiO amorphous phase detected by EXAFS and also the highest decrease of this phase after the oxidative treatments. As we have just described in the TPR data, the first peak has been ascribed by us to the reduction of this amorphous NiO phase (NiO → Ni). Therefore, if that was the case, the contribution of this peak to the total area must be related to the proportion of NiO detected by EXAFS and hence modified by the oxidative treatments. Fig. 8 shows the comparison of the TPR of the $LaNiO_3$-CM after these different treatments: (a) calcination; (b) O_2 (3%)–He 1073 K, 3 h and (c) O_2 (100%) 1073 K, 24 h. Two reducing different process can be still distinguished. The first of these two peaks was associated to the reduction of the NiO (amorphous phase) to Ni^0 and appears, independently of the treatment applied, in a similar range of temperatures (623–723 K), although its intensity clearly decreases with successive treatments (ca. 50%). The second process, at 723–823 K, was ascribed to the total reduction of the $LaNiO_3$ perovskite structure to $Ni^0 + La_2O_3$. On the contrary to the first reduction process, the intensity of this peak clearly increases with successive oxidative treatments. The values of H_2, determined from these profiles, were calculated as percentage of the total area. The peak at low temperature for the $LaNiO_3$-CM represents ca. 61% in "as calcined" sample, while after O_2 (3%) 1073 K for 3 h, its contribution is only 31%, being almost identical (29%) after the last oxidative treatment (O_2 (100%) 1073 K for 24 h). Taking this aspect into account, the presence of the NiO phase detected by EXAFS and the decrease detected in the ratio NiO/$LaNiO_3$ after the different oxidative treatments, we may suggest that the proportion NiO/$LaNiO_3$ depends on the method of synthesis but could be decreased by a deeper oxidative treatment. One possible relation between the methods of synthesis employed and the presence of the amorphous NiO phase could be the use of citric acid in the methods SPCM, CM and HT (which are the methods with higher amount of NiO). This citric acid could interact as a reducing agent, resulting species of Ni^{n+} lower than $n = 3^+$, being also reported that a defined ratio of nitrates/citric acid is crucial for getting the desired stoichiometry and a well defined crystallinity [45,46]. Previously we have associated the first peak of reduction to the NiO → Ni^0 process and the second one to the $LaNiO_3$ → Ni^0. After the more oxidative treatment we have observed by EXAFS the presence of only a phase of $LaNiO_3$, while in the TPR profile still presents a small and wide peak at low temperature. Therefore we have to reconsider the previous (and too simple assumption) that the first broad peak corresponds to the reduction of the NiO amorphous phase (to Ni^0), to a more complex situation that would involve two contributions: the reduction of NiO to Ni and a first step of the reduction of $LaNiO_3$ (clearly observed as separated processes in the b-profile of Fig. 8), without destroying the perovskite structure, as we have recently studied by TPR–XAS in situ experiments (Supplementary material).

Table 3
Crystallite size (calculated by XRD-Scherrer) of $LaNiO_3$-CM reduced after pre-treatments: air 873 K, 4 h; O_2 (3%)–He 1073 K, 3 h and O_2 (100%) 1073 K, 24 h.

$LaNiO_3$-combustion reduced after the pre-treatments:	Crystallite size^{XRD} (nm) Ni^0 (1 1 1), $\theta = 44.5^\circ$
Air – 873 K – 4 h	42
O_2 (3%) – 1073 K – 3 h	36
O_2 (100%) – 1073 K – 24 h	28

Due to the changes observed for the sample $LaNiO_3$-CM after the calcination treatments (by EXAFS, TPR and size of Ni – Table 3), the sample after O_2 (100%) treatment at 1073 K for 24 h was tested in dry reforming of methane and compared with the original one (calcined in air at 873 K), being the results represented on Fig. 9. It is possible to appreciate a great enhancement in the activity after the treatment more oxidative, reaching the methane conversion a value of ca. 80% in contrast with the much lower activity registered for the $LaNiO_3$-CM calcined in air. There is also an improvement in the ratio H_2/CO, nearby the theoretical value (H_2/CO = 1), for the sample treated in pure oxygen during 24 h.

As we have explained previously, $LaNiO_3$ phase is only a precursor of the active (Ni^0/La_2O_3) phase, produced either by a previous reduction or by its decomposition in the reactive mixture ($CO_2 + CH_4$). It is well accepted that Ni particle size, in the reduced form (Ni^0/La_2O_3), is one of the factor that affect the performance of these systems. Table 3 shows the size of the Ni crystallite (1 1 1) of samples "recalcined" after their reduction, with values calculated by applying the Scherrer equation to the diffraction peak at 44.5°. These data reflect a decrease in the size of the Ni (formed after reduction of $LaNiO_3$) when the pre-treatments of calcination are more oxidative (i.e. lower amount of NiO is present). The size varies from the 42 nm obtained for the as calcined in air sample to the 28 nm achieved after the treatment in pure oxygen during 24 h, near the optimum size 10–20 nm [40].

These results (EXAFS, TPR, size of Ni and DRM) relate the presence of an amorphous NiO phase with the catalytic results in DRM, and may explain the different activity reflected in the literature for this kind of material ($LaNiO_3$).

$LaNiO_3$-combustion reduced (20mg)	H_2/CO	T_{CH4}^{50} (K)
■ **Air-873 K-4h**	0.63	-
□ **O_2-100%-1073 K-24h**	0.92	1073

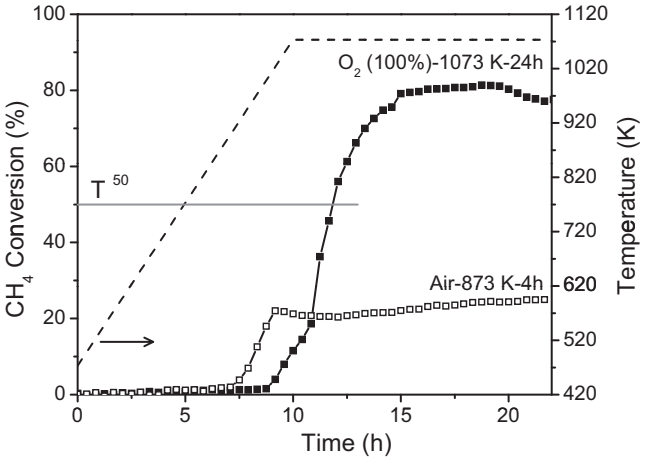

Fig. 9. CH_4 conversion, H_2/CO at 1073 K (t = 12 h) and temperature at 50% of CH_4 conversion ($T_{CH_4}^{50}$) for $LaNiO_3$-CM pre-reduced after treatments: air 873 K, 4 h and O_2 (100%) 1073 K, 24 h.

4. Conclusions

In the present work we have prepared $LaNiO_3$ by four methods, resulting samples with a crystalline $LaNiO_3$ rhombohedral phase and the presence of an amorphous NiO phase in different proportions that have been evidenced by EXAFS and TPR experiments. We propose that the quantity of NiO presents in the samples is related with the method of preparation employed but can be diminished with further oxidative treatment applied to the samples, being the NiO proportion lower when more oxidative treatment is applied. This lower amount of NiO amorphous phase is generally reflected in a higher conversion for DRM.

The TPR experiments present (for the 4 samples studied) two peaks. First peak is associated with the reduction of NiO to Ni^0 if this phase is present, together with a partial reduction of $LaNiO_3$ without destroying the perovskite structure (at 623–723 K), while the second peak (at 793–818 K) would correspond to the bulk reduction of $LaNiO_3$ to Ni^0.

The results presented for the characterization of the samples (metallic phase size, specific surface, reducibility, dispersion) together with the catalytic tests indicated that the $LaNiO_3$ prepared by the hydrothermal and spray pyrolysis methods have the most favourable properties for the DRM, but on the other hand, the sample obtained by combustion presents the lowest activity and worst properties as catalyst for dry reforming.

The higher presence of the NiO phase detected in the $LaNiO_3$-CM sample induces the formation of big Ni^0 particles after its reduction that present a low activity for DRM; however it is possible to improve the catalytic performance depending on the method of calcinations employed for $LaNiO_3$.

Acknowledgements

Authors want to express their gratitude to Spanish Ministry of Science and Education and Junta de Andalucia for approval and funding of research projects ENE2007-67926-C02-01 and P07-FQM-02774), and the PhD grants of R. Pereñiguez and V.G. de la Cruz. We also thank the staff of the SLS SuperXAS beamline and ESRF BM25 beamline; and to the SLS and ESRF facility for funding and helping with the XAS experiments.

Appendix A. Supplementary data

Supplementary data associated with this article can be found, in the online version, at http://dx.doi.org/10.1016/j.apcatb.2012.04.044.

References

[1] K. Tomishige, O. Yamazaki, Y. Chen, K. Yokoyama, X. Li, K. Fujimoto, Catalysis Today 45 (1998) 35.
[2] D.L. Trimm, Catalysis Today 49 (1999) 3.
[3] J.R. Rostrup-Nielsen, Studies in Surface Science and Catalysis 68 (1991) 85.
[4] I. Alstrup, N.T. Andersen, Journal of Catalysis 104 (1987) 466.
[5] S. Tang, L. Ji, J. Lin, H.C. Zeng, K.L. Tan, K. Li, Journal of Catalysis 194 (2000) 424.
[6] C. Batiot-Dupeyrat, G. Valderrama, A. Meneses, F. Martínez, J. Barrault, J.M. Tatibouët, Applied Catalysis A 248 (2003) 143.
[7] G.S. Gallego, C. Batiot-Dupeyrat, J. Barrault, E. Flórez, F. Mondragón, Applied Catalysis A 334 (2008) 251.
[8] N. Mota, R.M. Navarro, M.C. Alvarez-Galvan, S.M. Al-Zahrani, J.L.G. Fierro, Journal of Power Sources 196 (2011) 9087–9095.
[9] M.C. Álvarez-Galván, D.A. Constantinou, R.M. Navarro, J.A. Villoria, J.L.G. Fierro, A.M. Efstathiou, Applied Catalysis B 102 (2011) 291.
[10] E. Ruckenstein, Y.H. Hu, Journal of Catalysis 161 (1996) 55.
[11] S.M. Lima, J.M. Assaf, M.A. Peña, J.L.G. Fierro, Applied Catalysis A 311 (2006) 94.
[12] G.S. Gallego, F. Mondragón, J. Barrault, J.M. Tatibouët, C. Batiot-Dupeyrat, Applied Catalysis A 311 (2006) 164.
[13] G. Valderrama, M.R. Goldwasser, C. Urbina de Navarro, J.M. Tatibouët, J. Barrault, C. Batiot-Dupeyrat, F. Martínez, Catalysis Today 107–108 (2005) 785.
[14] C. Guo, J. Zhang, X. Zhang, Reaction Kinetics and Catalysis Letters 95 (1) (2008) 89.
[15] R. Pereñíguez, V.M. Gonzalez-DelaCruz, A. Caballero, J.P. Holgado, Applied Catalysis B 93 (3–4) (2010) 346.
[16] J.W. Nam, H. Chae, S.H. Lee, H. Jung, K.Y. Lee, Natural gas conversion V, Studies in Surface Science and Catalysis 119 (1998) 843.
[17] Z. Zhang, X.E. Verykios, Applied Cataysis A 138 (1996) 109–133.
[18] D. Trong On, S.V. Nguyen, S. Kaliaguine, Physical Chemistry Chemical Physics 5 (2003) 2724.
[19] E. Bontempi, C. Garzella, S. Valetti, L.E. Depero, Journal of the European Ceramic Society 23 (2003) 2135.
[20] H. Taguchi, S. Yamada, M. Nagao, Y. Ichikawa, K. Tabata, Materials Research Bulletin 37 (2002) 69–76.
[21] V.M. Gonzalez-Delacruz, F. Ternero, R. Pereñíguez, A. Caballero, J.P. Holgado, Applied Catalysis A 384 (2010) 1–9.
[22] E. López-Navarrete, M. Ocaña, Journal of the European Ceramic Society 22 (2002) 353.
[23] B. Ravel, M. Newville, Journal of Synchrotron Radiation 12 (4) (2005) 537.
[24] A.L. Ankudinov, J.J. Rehr, Phys. Rev. B 56 (1997) R1712; J.J. Rehr, R.C. Albers, Rev. Mod. Phys. 72 (2000) 621.
[25] M.C. Sánchez, J. García, J. Blasco, G. Subías, J. Perez-Cacho, Physical Review B 65 (1–9) (2002) 144409.
[26] P. Malet, A. Caballero, Journal of the Chemical Society, Faraday Transactions 84 (7) (1988) 2369.
[27] H. Wustenberg, Hahn, Inst. fur Kristallogr, Technische Hochschule, Aachen, Germany, ICDD Grant-in-Aid, 1981.
[28] M.A. Goula, A.A. Lemonidou, A.M. Efstathiou, Journal of Catalysis 161 (1996) 626.
[29] Y. Matsumura, T. Nakamori, Applied Catalysis A 258 (2004) 107.
[30] J.R. Rostrup-Nielsen, Journal of Catalysis 27 (1972) 343.
[31] W.L. Van Dijk, J.A. Groenewegen, V. Ponec, Journal of Catalysis 45 (1976) 277.
[32] G.H. Martin, M. Primet, J.A. Dalmon, Journal of Catalysis 53 (1978) 321.
[33] E.G.M. Kuijpers, A.J.H.M. Kock, M.W.C.M.A. Nieuwesteeg, J.W. Geus, Journal of Catalysis 95 (1985) 13.
[34] M. Che, C.O. Bennett, Advances in Catalysis 36 (1989) 55–172.
[35] J. Wei, E. Iglesia, Journal of Catalysis 224 (2004) 370.
[36] R.A. Van, Santen, Accounts of Chemical Research 42 (2009) 57.
[37] C. Henry, C. Chapon, S. Giorgio, C. Goyhenex, in: R.M. Lambert, G. Pacchioni (Eds.), Chemisorption and Reactivity on Supported Clusters and Thin Films. Towards an Understanding of Microscopic Processes in Catalysis, Kluwer Academic Publishers, Dordrecht, The Netherlands, 1997, pp. 117–152.
[38] S. Takenaka, S. Kobayashi, H. Ogihara, K. Otsuka, Journal of Catalysis 217 (2003) 79.
[39] Y. Li, B. Zhang, X. Xie, J. Liu, Y. Xu, W. Shen, Journal of Catalysis 238 (2006) 412.
[40] J. Zhang, H. Wang, A.K. Dalai, Applied Catalysis A 339 (2008) 121.
[41] T. Vaz, A.V. Salker, Materials Science and Engineering: B 143 (2007) 81.
[42] L. Huang, M. Bassir, S. Kaliaguine, Applied Surface Science 243 (2005) 360.
[43] M. Kuras, R. Roucou, C. Petit, Journal of Molecular Catalysis A: Chemical 265 (2007) 209–217.
[44] X. Wang, Y. Wei, J. Zhang, H. Xu, W. Li, Reaction Kinetics and Catalysis Letters 89 (1) (2006) 97.
[45] Y. Li, L. Xue, L. Fan, Y. Yan, Journal of Alloys and Compounds 478 (2009) 493–497.
[46] A. Mali, A. Ataie, Ceramics International 37 (2011) 2229–2236.